Gianclaudio Pinto
Daniel Cantero

NTNU
Norwegian University of Science and Technology

Modelling post-tensioned structures with DIANA FEM software

Trondheim – May – 2022

Report

NTNU
Norwegian University of Science and Technology
Faculty of Engineering
Department of Structural Engineering

ISBN: 978-82-7482-201-6

NTNU
Norwegian University of Science and Technology

Table of contents

1. Introduction

This report aims at providing additional information and insights for the numerical analysis of damaged post-tensioned concrete in a finite element analysis framework. The study focuses on modelling the behaviour of post-tensioned structures, especially when affected by partial or complete missing grout. The work was entirely carried out using the finite element program DIANA FEA BV. The present work is a research activity related to "*Bedre bruvedlikehold – DP2 Armeringskorrosjon – A4 Vedlikehold av spennarmerte konstruksjoner*" *(Better bridge maintenance – Corrosion – Maintenance of prestressed constructions)*, a project launched by the Norwegian Public Roads Administration (NPRA).

The purpose of this report is to investigate and to explore how to model numerically the presence of voids in post-tensioned systems. In finite element analysis frameworks, the possibilities of completing this task, range from local analysis on the interface surrounding the post-tensioned tendon to analysis on the reinforcement itself. The DIANA software allows to investigate in such a way, giving also to the user the possibility to decide the most suitable modelling technique to define the presence of damages along a tendon.

The body of this report consists in a brief introduction about the topic of the durability of post-tensioned structures and its main issues and characteristics. After this preliminary overview of the topic, the case of study is presented: a simply supported beam with a parabolic-shape tendon was designed according to EC2. In the central part of the report, the beam is then investigated numerically for various voids locations and the theory behind these numerical simulations is also provided. Finally, non-linear analyses were performed to investigate both the capacity and the cracking behaviour of the differently grouted configurations.

2. Durability of post-tensioned structures

Post-tensioned concrete structures are commonly adopted, in particular for bridges. The durability requirements of these structures are very strict, but the adoption of post-tensioning is still a good match for these requirements. Usually, post-tensioned concrete bridges are durable, and they do not require constant maintenance. However, if these structures are not properly designed, or constructed properly, severe deterioration conditions may arise [1]. The most common damages are corrosion, breakage of strands, section loss, voids, water infiltration and weak or compromised grout in the tendons. These deterioration conditions can be a real threat to the health of the structure. In particular, the presence of corrosion, if not treated properly in the early stages, could lead to an unexpected failure of tendons [2]. The scope of his report is limited only to the presence of voids due to the lack of grout inside the ducts.

The grouting of the tendons is made of chemically basic cement grout and it provides a passive environment (passive protection) around the bars or strands. It also serves the purpose to bond internally the tendons to the structure, creating the perfect conditions for the co-operation of concrete and the prestressing steel in each section. However, if the grouting is of poor quality, the durability of the tendons decreases. In particular, these damages can occur in several and particular regions in ducts, like for instance, near the anchorage region, which is one of the most critical parts of post-tensioning. Any damage concerning the grout has a major effect on the bonding properties affecting the section stiffness. If the grout is missing (partial or complete) between the strands and the duct, proper bonding conditions do not exist. In such cases the structure is weaker than expected and it does not behave as assumed in the design stage.

However, in some situations, tendons are not grouted and are left permanently unbonded. In particular, in this condition, the strands in the tendons are inside a plastic sleeve which is also filled with grease. Thus, the tendons remain unbonded from the surrounding concrete for the entire life of the structure. Unbonded systems, however, give less contribution to the ultimate strength of the structure and this is estimated to be approximately about 75% of that provided in bonded systems. This is because the strands are free to move locally relative to the concrete, not achieving strain compatibility between materials.

3. Case of study

The analysed case is a simply supported post-tensioned beam. The beam has a total length of 10 m, width of 0.4 m and height of 1 m. The prestressing reinforcement consist of 8 strands, half of them are prestressed on the left side and the other half on the right side. Each tendon has an area of 100 mm^2 (Ø8). The tendon layout is parabolic as displayed in Figure 1, where the eccentricity is e = 0 mm at x = 0 m and x = 10 m, while the maximum eccentricity is reached at mid-span with e = 350 mm at x = 5 m. The tendon depicted in the figure is the resultant tendon located at the centre of mass of the reinforcement, which can be used for design calculations and finite element analysis. This was used especially for 2D analysis and it is useful to have a faster overview of the mechanism of the post-tension. The initial force in each tendon is 106 kN (850 kN in total). Furthermore, neither longitudinal additional reinforcement nor stirrups were considered into the calculations, unless specified otherwise. The bending resistance of the beam was assigned only at the prestressed tendon, while the shear resistance was not considered neither with nor without shear reinforcement.

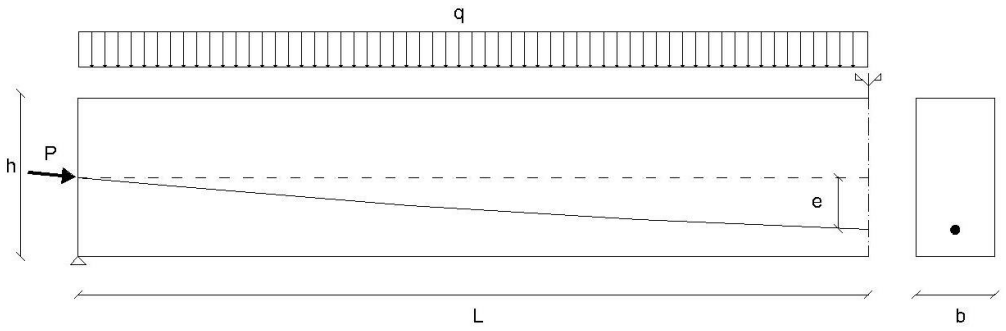

Figure 1: Beam layout

The concrete assumed in the calculation is a C45/55 with a tensile strength of 3.8 MPa. Concrete long-term deformations, such as creep and shrinkage, were calculated according to EN 1992-1-1(2004) [3]. The beam under examination is subjected to a uniformly distributed load *q* that was first assumed as 50 kN/m and then it was increased up until failure to observe a crack pattern formation in the finite element model. The case of study was designed entirely according to the Eurocode 2. Calculations for short, long-term losses and the design at both the serviceability and ultimate limit state were performed. The calculation helped to have a first insight of the behaviour of the beam (cracked or uncracked, the magnitude of loads and losses) and, especially, to set up the input parameters in the finite element software.

4. Finite element modelling

The main part of the work was carried out investigating and understanding the modelling approach for post-tensioned systems and all their possibilities within DIANA. Then the lack of

grout condition and its effect on the bonding properties was modelled. It is worth mentioning that in these systems, grouting and bonding, are concepts that cannot be separated and that are always present at the same time. Finite elements software available on the market have several and different approaches when it comes to the modelling of these systems. But in general, they are all unable to recognize or to distinguish a perfectly grouted situation from a damaged one. However, they can reproduce those real situations in terms of bonding properties. In particular, the bonding properties can be discretized along the interface located in between the active steel and the surrounding concrete. Other alternatives are modelling the tendons and the interaction with the concrete using springs or tying, or material and geometric properties already built-in in the software. Other publications, presented non-linear finite element formulations, i.e. Huang-Kang (2019) [4], based only on nodes, stiffness matrix and degrees of freedom, which can be used instead of the FEM software. Regardless of all the modelling techniques available in the literature, this work approaches the modelling problem of the post-tension only using the tools available in DIANA.

4.1. Theory Background

The modelling options available are the "embedded reinforcement" and the "bond-slip reinforcement". Post-tensioned (but also pre-tensioned) systems can be reproduced with these two options, which transfer all the characteristics of the pre- and post-tension directly and only to the reinforcement. The main difference between these two methods lies in the way in which the reinforcement element is computed in both situations.

In the embedded case, the reinforcements are fully embedded in the elements in which they are located, and relative slip is not allowed. Furthermore, the reinforcement is not represented with additional degrees of freedom and they have a truss-like behaviour with stresses and strain computed in the longitudinal direction only and from the displacement field of the mother element [5]. This definition implies perfect bond between the reinforcement and the surrounding material. However, as in a pre- and post-tension situation, the user can specify that the reinforcement is not bonded to the embedding elements. The embedded reinforcement relies on the concept of the internal virtual work which consists of two separate contributions. The stresses in the reinforcement and the concrete are calculated separately and split into two separate parts. This leads to a separate stress-strains relation for the reinforcement and the concrete. Unfortunately, the assumptions of the embedded tends to fail when the concrete enters the non-linear stage because the real bonding properties are not considered.

On the other hand, bond-slip reinforcement is internally modelled as a truss or a beam element and they are connected to the embedding elements by line-plane, line-shell, or line-solid interface elements. This option, in contrast to the embedded case, allows the user to calibrate the bonding properties of the reinforcement. Also, the interface element, which is included to calculate the slip, has a zero thickness. Both the embedded and the bond-slip reinforcement require specification of the material behaviour (linear or non-linear) but the latter requires also input parameters to describe the bond-slip interaction between the bar and the concrete.

The mechanism of the bond-slip is based on the concept of the structural interface elements. These elements correlate the forces acting on the interface to the relative displacement of the two sides of the interface, as shown in Figure 2.

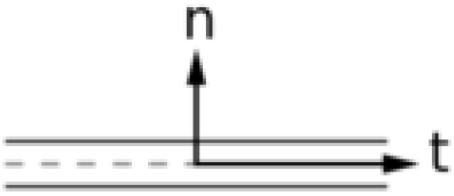

Figure 2: 2D configuration - interface element

The tractions present components in each direction: τ_n is the traction in the normal direction and τ_s and τ_t are the shear tractions. Also, the displacements are divided into normal relative displacement Δu_n and shear relative displacement Δu_t. In the software, the relation between the traction and the displacement is defined as follows in Eq. (1):

$$\begin{cases} \tau_n = k_n \, \Delta u_n \\ \tau_t = f_t \, (\Delta u_t) \end{cases} \quad \text{Eq. (1)}$$

which differentiating results in the expressions for the tangential stiffness coefficients, Eq.2:

$$\begin{cases} D_{11} = k_n \\ D_{12} = 0 \\ D_{21} = 0 \\ D_{21} = \dfrac{\partial f_t}{\partial \Delta u_t} \end{cases} \quad \text{Eq. (2)}$$

The relation between the normal traction and the normal relative displacement is assumed linear elastic, and the relation between the shear traction and the slip is a non-linear function. The input parameters of the bond-slip reinforcement will be described in more detail in the following paragraphs.

4.2. Post-tensioning

The case of study described in Section 2 was modelled in the software in different ways. As previously said, the post-tension system can be modelled through both the embedded and the bond-slip reinforcement, but also anchorages and other features can be included if the purpose of the work requires it.

Table 1 provides an overview of the models created in DIANA.

Table 1: Features of DIANA models

	Embedded reinforcement		**Bond-slip reinforcement**	
	2D	**3D**	**2D**	**3D**
Beam elements	*Q8MEM*	*CHX60*	*CQ16M*	*CHX60*
Number of tendons	1	8	1	8
Anchorage device	-	-	2 blocks 100×100×10mm	8 blocks 30×30×20mm

The *Q8MEM* is a 4-node quadrilateral plane stress element with two translational degrees of freedom per node, and it is based on Gauss integration and linear interpolation. The *CQ16M*, instead, is an 8-node quadrilateral plane stress with 8 nodes. The *CHX60* is a 20-node isoperimetric solid brick element used in the 3D models.

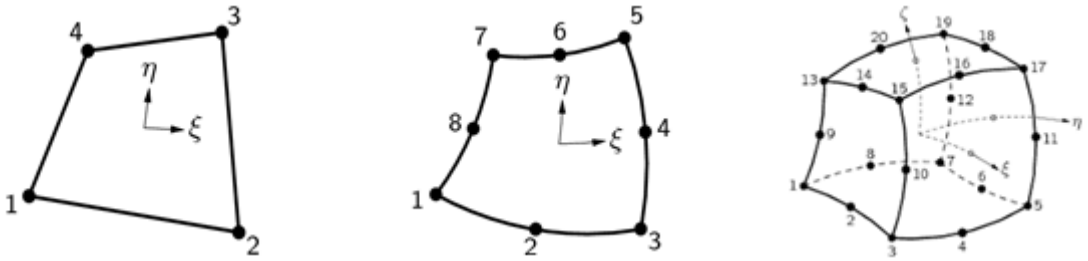

Figure 3: Element types

As depicted in Table 1, several models have been created. In the embedded case a first order mesh (*Q8MEM*) was adopted to avoid numerical problems in the calculation of the post-tension losses along the tendon. All the finite element models are like the one depicted in Figure 4. Embedded reinforcement models do not require anchorage strategies to represent the tendon ends. The bond-slip models have been modelled either with or without the presence of the anchorage devices. In the first case, the anchorage system is modelled, and the tendon is anchored to it, while, in the second case, the anchorage is not modelled, and the tendon is anchored to the ends of the beam. Also, in the first scenario, the reaction forces developed by the post-tensioned are applied to the anchorages, while, in the second scenario, directly to the beam.

For all the models, the element size has been calculated according to the guidelines for non-linear finite element analysis [6]. For reinforced concrete members, the recommended element size should be less than $\min\left(\frac{L}{50};\frac{h}{6}\right)$ for 2D modelling and $\min\left(\frac{L}{50};\frac{h}{6};\frac{b}{6}\right)$ for 3D modelling, where *h* is the depth, *L* the span, and *b* the width of the beam. The maximum values for 2D and 3D are respectively 166 mm and 66 mm and, in order to avoid jumps from one element to another (coarse mesh), a fine mesh of 25 mm was chosen. This element size ensures the stress field to be homogeneous.

The embedded reinforcement is the main used tool in all the finite element analyses. Thanks to its theoretical formulation, the user can model the reinforcement in concrete in a very easy way. In DIANA v10.4 the user can model the post-tension (or pre-tension) in combination with the embedded reinforcements. The mechanism of the post-tension is reproduced through the definition of an external load applied to the reinforcement. The tensioning requires just the selection of the reinforcement elements and the definition of some parameters. The main parameters are the tensioning force *P*, the friction coefficient μ, the wobble factor φ whose unit is (1/*L*) and the retention of the anchorage which is usually 6 mm. Also, it must be specified how the tendons are anchored, i.e., if the tendons are tensioned from both ends or one end is tensioned and the other is anchored.

The losses calculated with this tool are the ones due to the friction and the anchorages. In particular, the friction losses are calculated according to the MC1990 (European CEB-FIP Model Code 1990[7]) scheme.

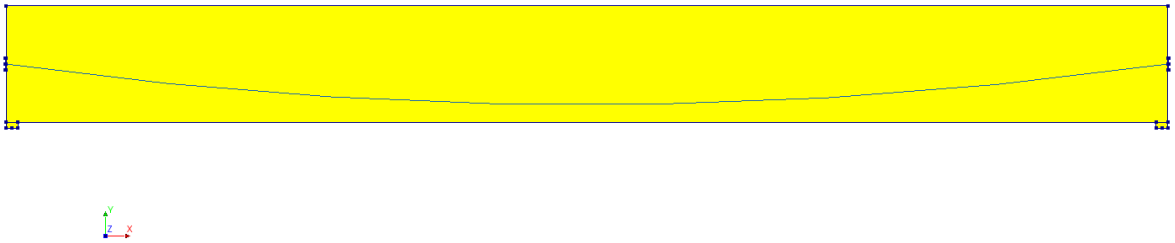

Figure 4: 2D model - bond-slip reinforcement

The bond-slip models, as depicted in Table 1, were built differently from the embedded ones. These models also include the anchorages at the ends of the beam. The post-tension in the bond-slip reinforcement (in contrast to the embedded case in which the "post-tension load" tool is available) is achieved adjusting the bonding properties of the tendons.

To summarise, the main aspects to control are the tensioning force in the tendon, the bonding properties and the anchorage of the tendon. The tensioning force must be applied at the ending vertex of the tendon and it requires also the definition of the components in *x*- and *y*- direction, since the force is inclined by the angle α, defined as $\frac{4e}{L} = 0{,}14$.

4.3. Bond-slip reinforcement - bonding properties of interface

The bonding properties of the interface are the key parameters of the bond-slip model. As described in Section 3.1, the relationship between stress and strain is set through the linear stiffness moduli. The linear stiffness moduli are D_{11}, D_{22} and D_{33}, where :

- D_{11} (*DSSX*) sets the relation between the shear traction τ_{sx} and the shear relative displacement Δu_{sx} in the reinforcement x direction. This is also called the shear stiffness modulus.
- D_{22} (*DSNY*) sets the relation between the normal traction τ_{ny} and the shear relative displacement Δu_{ny} in the reinforcement y direction. This is also called the normal stiffness modulus.
- D_{33} (*DSNZ*) sets the relation between the normal traction τ_{nz} and the shear relative displacement Δu_{nz} in the reinforcement z direction. This is only applicable for shells or solids. If this parameter is not specified, the value of D_{22} will be used instead.

The adoption of these parameters leads to a linear correlation between stress and strains. However, it is also possible to use a non-linear relation, which can be defined using the bond-slip laws available in DIANA. The bond-slip law proposed by Dörr (Figure 5) was used for the analysis. The law, which is called "*cubic function*", is defined by a polynomial relation between shear traction and slip (Eq. 3). Dörr sets a limit beyond which the bond stress remains constant and only the slip is allowed to increase.

$$t_t = \begin{cases} f_t \left(5\left(\frac{\Delta u_t}{\Delta u_t^0}\right) - 4.5\left(\frac{\Delta u_t}{\Delta u_t^0}\right)^2 + 1.4\left(\frac{\Delta u_t}{\Delta u_t^0}\right)^3 \right) & if\ 0 \le \Delta u_t \le \Delta u_t^0 \\ 1.9\, f_t & if \Delta u_t \ge \Delta u_t^0 \end{cases} \qquad \text{Eq. (3)}$$

The parameters of this bond-slip law are the maximum bond stress t_t and the slip Δu_t^0 which are respectively set as 1.9 times the tensile strength of concrete, 7.2 MPa, and 0.06 mm.

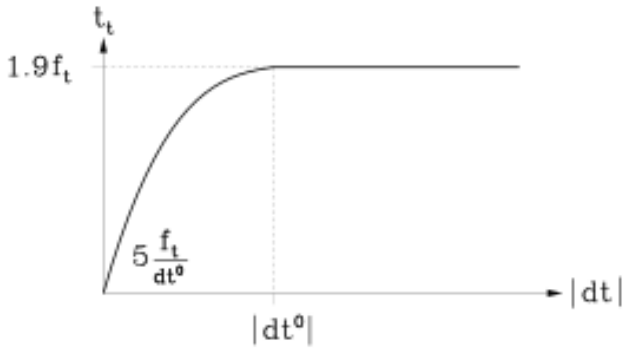

Figure 5: Dörr cubic function

Thus, these are the two main options which allow the user to define entirely the bonding properties of the interface of the bond-slip reinforcement. Practically, it can be done either by defining the stiffness parameters D_{11}, D_{22} and D_{33}, so a linear elastic approach, or using one of the bond-slip laws available in DIANA, which leads to a non-linear approach. It must be mentioned that this non-linear approach, which uses the several bond-slip laws, available in DIANA, defines exclusively a non-linear behaviour for the shear stiffness. Thus, the user must always define the normal stiffness and the shear stiffness, and the latter can be defined either by a linear or a non-linear approach. For instance, using both methods would not lead to numerical issues or any other kind of conflicts, because the software will automatically detect the bond-slip law given by the user and it will also calculate the D_{11} related to it. In fact, this stiffness is simply the shear elastic stiffness of the bond-slip law which, in this case, using Dörr's law, is calculated as $\frac{5f_t}{\Delta u_t^0}$, as depicted in Figure 5.

Furthermore, being the bond-slip a mechanism acting mainly along with the interface in the tangential direction, the normal elastic stiffness D_{22} assumes a secondary role and it is not usually taken into account during the analysis. However, there are situations in which the normal elastic stiffness D_{22} becomes relevant. If this happens, then the "linear approach" with the elastic stiffness and the "non-linear" approach with the bond-slip laws are directly linked. The independence of the two approaches gets lost because of the geometry of the tendon. In particular, for curved reinforcement bars, like the tendons for the post-tension, both the normal

and the shear stiffness are relevant. This does not concern the case with straight reinforcement bars, like in the case of pre-tension or pull-out tests.

The previous considerations led to only two possible approaches for defining properly the bonding properties of the tendon:

- Linear approach, as described previously, by defining both the normal and shear elastic stiffness, D_{22} and D_{11}.
- A mixed approach, by defining the normal elastic stiffness D_{22} and the bond-slip law. In this way, the bonding properties are still defined in the normal and tangential direction to the interface.

Both these approaches were tested for this project but the "*mixed approach*" was chosen and used throughout this report. The choice was influenced by the uncertainty in the values of the normal and the shear stiffnesses to use. In fact, after a thorough literature review, it was noted that the definition of these two parameters is neither well documented nor properly explained. However, even though the uncertainty linked to this topic is relevant, the interpretation and the nature of these two stiffnesses can be explained easily. *DSSX*, the shear stiffness, is interpreted as the slope of the bond-slip curve at zero slip, as briefly mentioned earlier. The value for the shear stiffness, considering the cubic bond-slip formulation, is calculated at the plateau of the bond-slip curve which corresponds to a slip value of 0.06mm. Thus, according to also to Figure 5, the value is estimated as in Eq. (4). The values of this stiffness can be different if other bond-slip formulations are used, i.e. Model Code 2010.

$$DSSX = \frac{5f_t}{\Delta u_t^0} = 600 \ \frac{\frac{N}{mm^2}}{mm} \qquad \text{Eq. (4)}$$

DSNY, the normal stiffness, is interpreted as the stiffness related to the crushing of the concrete by the reinforcement bar [8]. This is assumed to be constant regardless of the bond-slip curve. The value of DSNY is estimated according to Hendriks and [8]. Figure 6 depicts a reinforcing bar surrounded by concrete and the normal stiffness is presented in a way that resembles its earlier definition (i.e. *"the concrete resistance to the reinforcement penetrating and crushing the concrete "*). According to this consideration, the formulation of the normal stiffness can be written as:

$$DSNY = \frac{E_c}{2R} * 10^3 \ \frac{\frac{N}{mm^2}}{mm} \qquad \text{Eq. (5)}$$

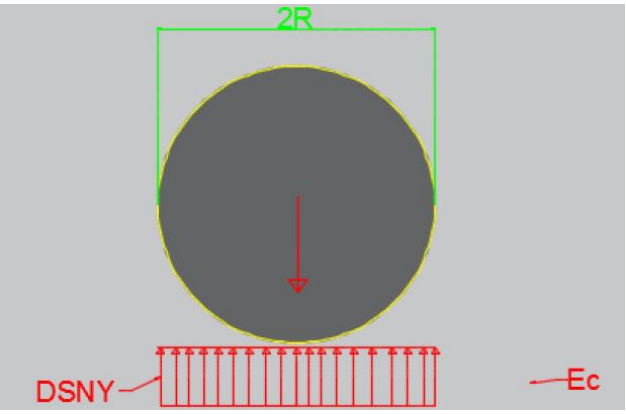

Figure 6: Definition of DSNY [8]

However, another formulation for the tangent and normal stiffness is available. The DIANA FEA support centre suggests a guideline for the identification of the most reasonable values for these parameters. In particular, the guideline suggests a tentative formulation [9], described as follows:

- Consider the average element size in the mesh, I_e.
- Consider an elastic modulus which is somewhat in between the values of elastic moduli of the elements surrounding the interfaces. Let this be denoted by E.
- Calculate the normal stiffness, K_n (*DSNY*), as: $100 \sim 1000 \cdot \frac{E}{I_e}$
- Compute the value of the shear stiffness, K_t (*DSSX*), by dividing K_n by 10 or 100.

Thus, to summarize, the main choices of calculation for the normal and the shear stiffness are:

- *DSSX* calculated according to Eq. (4) and DIANA guideline [9].
- *DSNY* calculated according to Eq. (5) and DIANA guideline [9].

The resulting values for each approach are showed in Table 2 and Table 3.

Table 2: Normal stiffness DSNY

Formulation		**DSNY**
		$I_e = 25\ mm$
DIANA guideline [9]	$E = \frac{(E_c + E_p)}{2}$	$4{,}63 \cdot 10^5 \frac{N}{mm^3}$
DIANA guideline [9]	$E = E_c$	$1{,}45 \cdot 10^5 \frac{N}{mm^3}$
Hendriks (eq.5)	$E = \frac{E_c}{2R} * 10^3$	$1{,}14 \cdot 10^5 \frac{N}{mm^3}$

In these calculations, following the DIANA guidelines, the factor 100 was chosen first to find K_n , and then divided by 10 to find K_t. This option helped to prevent the values of the stiffness moduli from being too high. With these factors the normal stiffness has the same order of magnitude as the elastic stiffness of the concrete. Furthermore, the second rows of the Tables 2-3 show the calculations made when using only the concrete stiffness. In these cases, the "elastic modulus" of the interface is calculated only using the concrete stiffness and no longer as an average of the moduli of concrete and steel.

Table 3: Shear stiffness DSSX

Formulation		DSSX
		$I_e = 25\ mm$
DIANA guideline [9]	$E = \frac{(E_c+E_p)}{2}$	$4{,}63 \cdot 10^4 \frac{N}{mm^3}$
DIANA guideline [9]	$E = E_c$	$1{,}45 \cdot 10^4 \frac{N}{mm^3}$
Eq.4	$\frac{5f_t}{\Delta u_t^0}$	$600 \frac{N}{mm^3}$

It is worth mentioning that the calculation procedure as stated above is merely a guideline and presented here as an overview of the possible calculations and outcomes. However, the final choice of the values should be made only after the results seem to be satisfactory. Indeed, in this work, as stated before, a linear approach with the values of the normal and the shear stiffness (Table 2-3), and, a mixed approach, with the normal stiffness values (Table 2) and the cubic bond-slip law, were both used. Several attempts were made with different values of *DSNY* and *DSSX*, but, in the end, the most suitable and reliable option was the mixed approach with *DSNY* = $1.45 \cdot 10^5$ N/mm^3 and the cubic bond-slip law (τ = 7.2 MPa and Δu_t^0 = 0.06 mm). In particular, the choice of this particular value of normal stiffness was due to the fact that using moderately higher value, such as $4.63 \cdot 10^5$ N/mm^3, led to significant losses of the prestressing force along the tendon. Finally, it is important that the user decides a value of normal stiffness that is not too small, i.e. equal to 0 N/mm^3, and not too high, i.e. equal to $1 \cdot 10^9$ N/mm^3, to avoid numerical errors, like depicted in Figure 7. The first scenario with DNSY equal to 0 led to the abrupt end of the analysis. Also, a peak in stress of $2.32 \cdot 10^6$ MPa can be observed in Figure 7a. The second case led instead to have the entire tendon over-constraint along its length, except the anchorage zones.

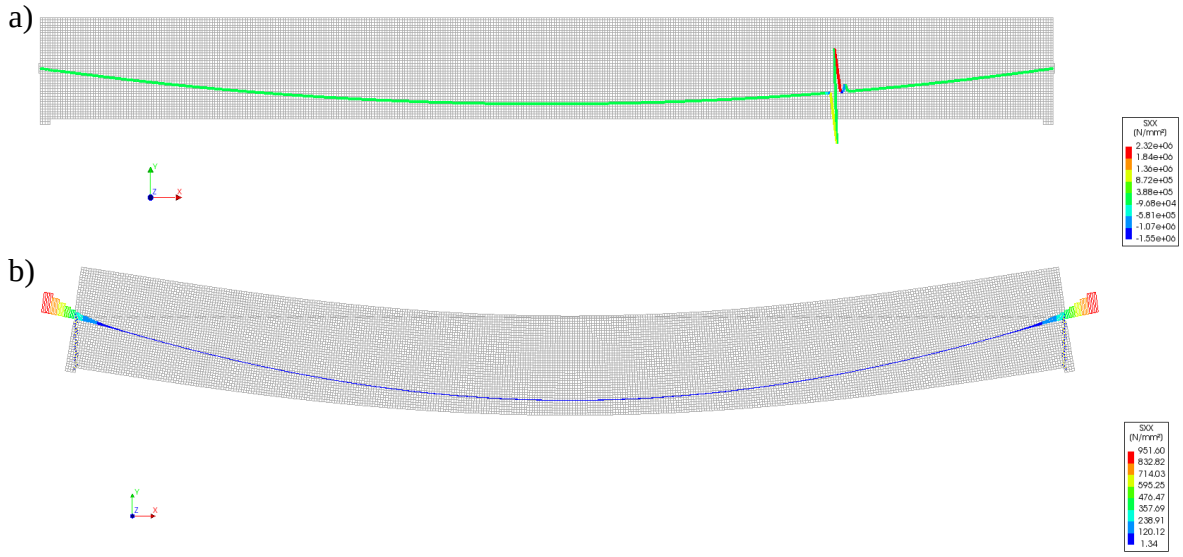

Figure 7: Numerical errors - a) DSNY =0 N/mm^3
b) DSNY = $1 \cdot 10^9$ N/mm^3

In a curved or parabolic shaped tendon, the uncertainty related to the value of the shear stiffness modulus can be overcome by using the bond-slip law, while the normal stiffness value has to be chosen carefully and calibrated. In this work, the calibration was not performed entirely, and the most suitable value was found based solely on the approximation of the distribution of

the prestressing force along the tendon. It was compared to the analytical calculation and to the distribution obtained from the embedded model. Also, note that the procedures suggested by DIANA are all dependent on the element size (i.e. Table 2-3,element size used=25 mm) while the procedure by Hendriks's [8] is based only on the concrete stiffness and on the geometry of the reinforcement. Furthermore, in the case of a coarse mesh, the DIANA procedure could lead to a very high values of the stiffness parameters.

4.4. Analysis

After all the parameters necessary for the bond-slip reinforcement were set, the analyses of the models were carried out. Both linear and non-linear analyses have been performed as load-step analysis. The linear analysis helped to check that all the parts and characteristics of the models worked correctly. Also, in the linear analysis, using the composed line tool provided by DIANA, the axial and shear forces, and the bending moments have been proved to be in accordance with the analytical calculations. The non-linear analyses were carried out in phases following the real procedure of post-tensioned beam. Theoretically, the post-tension is divided into three stages, as depicted in Figure 8:

- Concrete is cast and cured.
- Tensioning and anchoring of the tendons. The tendons lie in the duct without the presence of the grouting. Friction losses take place along the tendon. The prestress is transferred.
- The grouting is poured into the duct. The concrete and steel start to work together. The effects of the post-tensioning are active.

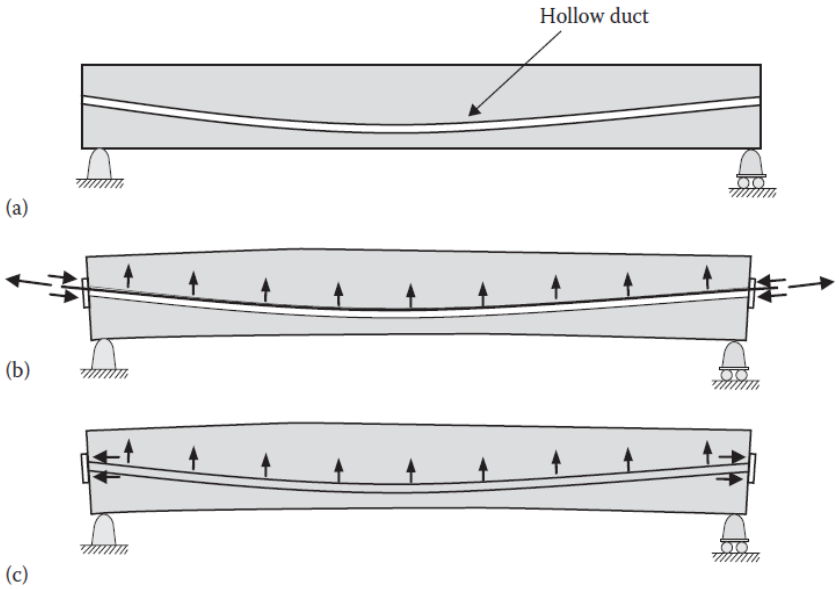

Figure 8: Post-tensioning stage: (a) Concrete cast and cured. (b) Tendons stressed and prestress transferred. (c) Tendons anchored and subsequently grouted [10]

It is possible to reproduce these stages in the non-linear analyses with both modelling alternatives, namely embedded model and bond-slip reinforcement model. The embedded, as stated previously, is more suited for checking a design at SLS and ULS. However, in the non-linear analysis it is possible, using the "physical non-linear properties", to assign bonding properties to the reinforcement. In the un-grouted phase, the reinforcement is not bonded while in the grouting phase, the bonding is achieved. The embedded option was used only for

comparison and not to pursue the object of this project, due to its inability to represent a damaged situation in the tendon. Thus, all the further considerations and evaluations are carried out only with reference to the bond-slip reinforcement model. In the bond-slip reinforcement model, the non-linear structural analyses were carried out differently as for the embedded model. The “phased analysis” helped to define each stage of the construction phase for the post-tensioned beam.

The phased analyses are a useful tool for modelling the different stages of construction. The effects of construction history and the critical construction stages can be determined. A phased analysis comprehends several calculation phases. Between each phase the finite element model changes by the addition or the removal of elements and constraints. In each phase a separate analysis is performed by the software, in which the results from previous phases are automatically transferred and used as initial values. Typical results are stresses, deformations, potentials, velocities etc. The start of each phase can include the input of the model part which is added; thus, the model may change from phase to phase. For instance, in each new phase, elements and reinforcements may become active or inactive at the users' request, or supports may be removed or added [5].

The aspects of the model that have been modified from phase to phase are the tying and the bonding properties of the prestressed steel. The tying and the bonding properties ensure that the model works as expected during each phase.

The phased analysis of the post-tensioning beam with the bond-slip reinforcement was performed as follows:

- Phase 1 - Calculate the pre-stresses in the tendon with no bonding conditions with concrete.
- Phase 2 - Calculate the model with bonding conditions with concrete.
- Phase 3 - Calculate the model with bonding conditions and service and/or additional loads.

Furthermore, to decrease the complexity of the model and the amount of data, Phase 2 and Phase 3 were treated as a single phased analysis. This was done because, the second phase defines the transition between phase a-b and c, Figure 8, and so, it might be useless to define additional phased analysis after that. This choice does not affect the results and it is still in accordance with the real behaviour of an actual post-tensioned beam. The analysis of a post-tensioned system requires just two phased analysis which make possible to change the bonding conditions of the tendons. Similarly, additional phases can be added if other phenomena need to be modelled.

The main loads acting on the models, whether on the embedded and the bond-slip reinforcement model, are the self-weight of the beam and the uniform distributed load. As stated previously, the post-tension load is defined differently in the embedded and the bond-slip model. The most important difference between the two models is the presence of the reaction forces at the anchorages in the bond-slip reinforcement model. Indeed, in the bond-slip, the post-tension load is defined as a force, with magnitude and direction, acting on the outer vertex of the tendon and the anchorage reactions are defined as a force system acting on the anchorages, with the same magnitude of the prestressing force but with opposite direction.

The load combinations used to perform the phased analysis for the bond-slip model are defined as follows:

- Load combination 1: Self weight + Post-tensioning forces + Reaction forces.
- Load combination 2: Self-weight only.
- Load combination 3: Additional load (uniformly distributed load q).

All the load combinations were defined with load factors equal to 1. The load combination 2, used in the second phase of the analysis, ends the process of the transfer of the post-tension to the structure. After that, all the load combinations used in the analysis act on a fully cast post-tensioned beam. A complete overview with all the details and characteristics of the model for each phase of the phased analysis, is given in Table 4.

Table 4: Non-linear phased analysis

	Phase 1	**Phase 2**	
Analysis type	Load step	Start step	Load step
Load	Load combination 1	Load Combination 2	Load Combination 3
Bonding properties	un-grouted	grouted	grouted
	$DSNY = 1{,}45 \cdot 10^5 \frac{N}{mm^3}$ $DSSX = 0\ N/mm^3$ $\tau = 1 \cdot 10^{-10}\ MPa$ $\Delta u_t^0 = 0.06\ mm$	$DSNY = 1{,}45 \cdot 10^5 \frac{N}{mm^3}$ $DSSX = 0\ N/mm^3$ $\tau = 7.2\ MPa$ $\Delta u_t^0 = 0.06\ mm$	$DSNY = 1{,}45 \cdot 10^5 \frac{N}{mm^3}$ $DSSX = 0\ N/mm^3$ $\tau = 7.2\ MPa$ $\Delta u_t^0 = 0.06\ mm$
Tying	Deactivated	Activated	Activated

Table 4 describes the methods used for the non-linear analysis, the loads, the bonding properties and the presence of the tying for each phase. All the steps in the phased analysis have been performed using the load stepping, except for the so-called “start step” in the first stage of the second phase. As stated before, the phased analysis allows the user to investigate the behaviour of the model throughout its entire evolution. In particular, the start step helps the software to recognize the instructions to be taken in the transfer from Phase 1 to Phase 2. The start step evaluates the initial state of the model before the execution of the load or time step. This command also balances the external forces, which are defined by the load command, and the internal forces, which are defined by the stresses in the elements. Stresses and strains are always transferred from phase to phase, but the external loads are not. Thus, the external load considered is self-weight only. In Phase 2 the bond-slip model with null strength parameters are changed to the one with real values and jacking forces are released. Thus, for this second phase:

- mesh size remains the same,
- supports remain the same,
- tendons’ bonding properties are changed,
- tying is introduced.

It is important to note that the change in the bonding properties of the tendon from Phase 1 to Phase 2 is because, first, the tendon is not bonded or grouted, and then it is fully bonded and grouted. Furthermore, in Phase 1, for defining the bonding properties, as stated previously, a “mixed approach” was used. The normal stiffness *DSNY* is big enough to ensure that friction losses develop along the tendon, while the shear behaviour, controlled and defined by the

Dörr's cubic law, is set to very small bonding stress, close to zero but not zero to avoid numerical problems. When the grouting is poured into the duct, the bond is established. The bonding properties in Phase 2 present the same values for the normal stiffness, while the cubic law shows the real values of the bonding stress. Once the Phase 1 is over, all the calculations of the relative displacement and stress between the active steel and the concrete, in the shear direction, are reset and the calculations start from the origin in the new bond-slip law of the second phase. This option is used because, due to the pulling force in the tendon in the first phase, an amount of slip is obtained. This slip shall not be considered after the bonding condition with concrete in Phase 2.

In a phased analysis using the bond-slip reinforcement it is only possible to modify the material properties while changes in geometrical properties (location, cross-section) are not allowed. Furthermore, since a change in material properties (bonding properties) was made, also the stiffness matrix of the truss elements of the bond-slip reinforcement was renewed by the program from Phase 1 to Phase 2.

In the second phase, the tyings are also introduced. They are essential elements to materialize the post-tension since they help to constrain the ends of the tendon to either the anchorage or the ends of the beam. Tyings are linear dependences between nodal variables that are defined in the geometry and passed to the mesh. The tyings are mainly specified through master nodes and slave elements (solids, line, faces or points). However, these elements must be formulated and placed correctly and with care. In particular, tyings depend on the degrees of freedom that are actually present in the real system to model, in this case, the anchorages, and, thus, they need to be modelled with caution. If the applied tyings are physically meaningless, this results either in unstable models due to the absence of equilibrium and/or inexplicable results [11].

When a model with tyings is created, it is recommended to check the moment equilibrium condition as follows:

- Step 1: Perform a linear elastic analysis of the model with one or more load cases.
- Step 2: From the results, consider the reaction forces in table view.
- Step 3: Copy the reaction forces along with the nodal coordinates into a spreadsheet.
- Step 4: Calculate the moments of each section.
- Step 5: Compare the calculated moments with the ones listed in the analysis output file (*.out).

These steps were performed for the analysis both in 2D and 3D and it was noted that the moment equilibrium conditions were satisfied, and the results were reliable. Then, several non-linear analyses were performed on different models with or without anchorages and models with one tendon or two tendons. Each model has its characteristic and considerations about the results. In order to pursue the object of this project, the bond-slip model with two anchorages and one tendon was analysed closer. Naturally, all the models created have been analysed in the following way, but for simplicity, only this one will be described and showed below.

The analysed model is depicted in Figure 8a showing the anchorage. The absence of these elements would not avoid the use of tying of the tendon to the concrete in the second phase, but it would neglect the anchorage losses in the first parts of the tendon. To overcome this, it is still possible in the bond-slip reinforcement to assign the anchorage length to the tendon to have the losses calculated.

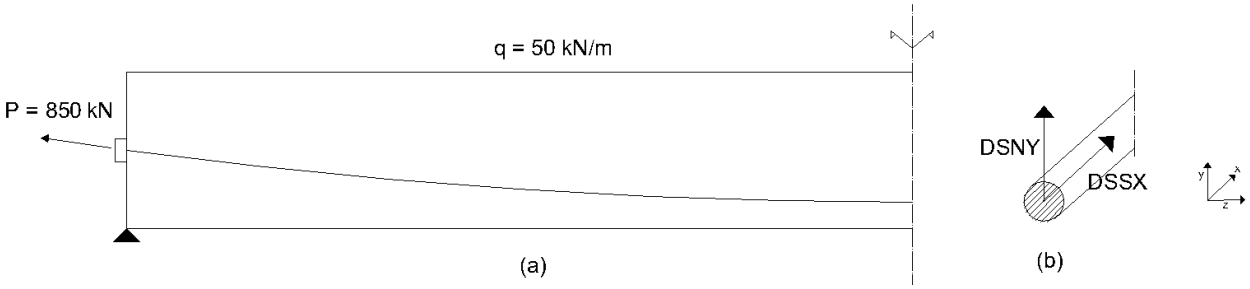

Figure 9: (a) Bond-slip model (b) Normal and shear stiffness

As described in the previous sections, the lack of grouting in the duct could be considered as a damaged situation. There is only one way that these damage situations can be reproduced in a finite element software like DIANA, and this is by modifying the bonding properties of the bond-slip interface.

The representation of a damaged situation in the post-tension system was defined through a change in the bonding properties and, thus, in the parameters of the bond-slip interface. The change of these parameters was based on the consideration that in a "damaged" section of the structure, the severe grouting conditions allow the presence in the normal and tangential direction of relative displacements. Furthermore, the tendon is not properly constraint anymore in the duct and the full strain compatibility between the concrete and steel cannot be reached, as displayed in Figure 10 [12].In the figure, is possible to observe an example of what stated previously: the lacking of grouting leaves the tendon completely disconnected from the duct allowing so, relative displacement in the two directions, and, severe corrosion conditions.

Thus, considering the finite element environment, the difference between a grouted (good bonding properties), and a damaged situation (poor bonding properties) resides in the behaviour of the tendon in the two directions, normal and tangential (Figure 9b).

Several studies were carried out to find out the most reliable values for the normal and the shear stiffness to represent a damaged situation. At the end, it was concluded that the stiffnesses in the two directions should have such small values that the tendon behaves like there is almost no resistance around it. It can be observed that the mixed approach, used to describe the different stages of the post-tensioning process (Table 4), presents in the first stage a high value for the normal stiffness, while on the shear direction this was controlled and defined by the cubic law, which presented values close to the origin. Thus, for the damaged behaviour, it was assumed that the best choice was to decrease the value of the normal stiffness, *DSNY*.

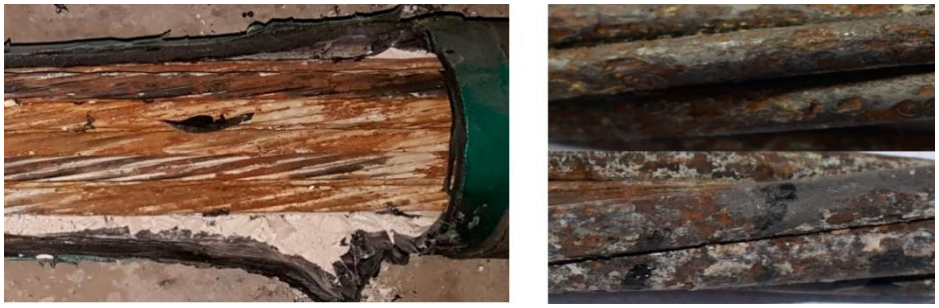

Figure 10: (Left) Imperfect grout filling; (Right) corroded internal strands [12]

The selection of the right value of *DSNY*, given the complex nature of the parameter itself and the mechanism to represent, was chosen to be greater than 0 and smaller than the actual value

$1.45 \cdot 10^5$ N/mm^3. The value chosen for the normal stiffness *DSNY* was 10 N/mm^3. This was a strong assumption since no experimental or analytical considerations are behind it. However, this value was deemed appropriate since a zero value led to numerical problems (tendon entirely disconnected from the model) and a value greater than $1.45 \cdot 10^5$ N/mm^3 caused an anormal level of constraint of the tendon in the model, as in Figure 7 (The tendon is so constraint by the surrounding concrete that the prestressing force is not transferred from end to end and, resulting in a behaviour different than a post-tensioned system). The parameters of the bond-slip used for each phase of the analyses are displayed in Table 5.

Theoretically, this stiffness parameters could be correlated to the level of grouting in the duct. This could be established through an experimental result under laboratory conditions. But this is out of scope of the present study. Therefore, the value previously cited was assumed to be the best option for a situation with severely damaged grouting or lack thereof.

Table 5: Different grouting/bonding conditions

Bonding properties	**Phase 1**	**Phase 2**
Grouted (good bonding/grouting conditions)	$DSNY = 1{,}45 \cdot 10^5 N/mm^3$ $DSSX = 0 \ \ N/mm^3$ $\tau = 2 \cdot 10^{-5}\ MPa$ $\Delta u_t^0 = 0.06\ mm$	$DSNY = 1{,}45 \cdot 10^5\ N/mm^3$ $DSSX = 0 \ \ N/mm^3$ $\tau = 7.2\ MPa$ $\Delta u_t^0 = 0.06\ mm$
Damaged (poor bonding/grouting conditions)	$DSNY = 1{,}45 \cdot 10^5 N/mm^3$ $DSSX = 0 \ \ N/mm^3$ $\tau = 2 \cdot 10^{-5}\ MPa$ $\Delta u_t^0 = 0.06\ mm$	$DSNY = 10\ N/mm^3$ $DSSX = 0 \ \ N/mm^3$ $\tau = 1 \cdot 10^{-10}\ MPa$ $\Delta u_t^0 = 0.06\ mm$

As displayed in Table 5, Phase 1 is identical for both situations while in the second phase the two grouting conditions are represented by different parameters.

After all the bond-slip properties have been set up, the attention was moved on how to discretize the tendon. Usually, the lack of grouting occurs near the anchorages or at mid-span of the structure. Therefore, it was decided to assume three different and simple configurations that somehow could have covered the multiple possible scenarios. In Phase 2, the configurations are defined as follows and depicted in Figure 10:

- (a) Tendon entirely grouted (good bonding/grouting conditions).
- (b) Tendon entirely damaged (poor bonding/grouting conditions).
- (c) Tendon divided into multiple parts of equal length with alternating both good and poor bonding conditions.

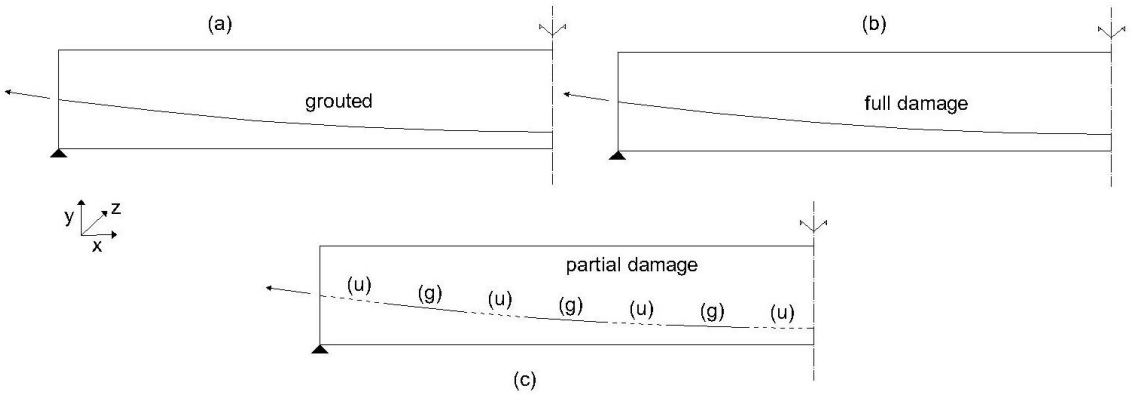

Figure 11: Configurations: (a) grouted, (b) full damage and (c) partial damage

These configurations have been analysed and the results are reported in Table 6, Table 7 and Table 8. The displayed results are the maximum vertical displacement δ, the maximum prestressing force in the tendon *P*, the interface relative displacements and the total traction along with the reinforcement, respectively *DUSx* and *STSx*. The maximum vertical displacement δ is calculated at midspan x = 5 m, the maximum prestressing force *P* both at midspan and at the ends of the tendon (x = 0 m and x = 10 m), and the relative displacement and the total traction, *DUSx* and *STSx*, also, at the ends of the tendon.

It can be observed that the results of the different configurations show only small differences. In particular, the maximum vertical displacements are almost identical for all the configurations in the first phase and the first load step of the second phase. Furthermore, it can be observed that the "full damage model" (Figure 10b and Table 7) exhibits, as expected, a vertical downwards displacement of 3mm, slightly larger than 2,98mm of the entirely grouted model. This is because slightly smaller stiffness of the damaged model. Also, the partial damage model shows a value of vertical displacement, equal to -2,99mm, almost in the middle of the other two models. The configuration of the partial damage model (Figure 10c and Table 8) was changed many times, increasing, decreasing, or moving the damaged parts but with no evident conclusions that could have led to parametric analyses.

Furthermore, the prestressing force in the tendon seems to show few differences too. The differences can be observed in the second load step of the second phase in which the uniformly distributed load is acting. In the grouted model (a) the value of the force at the end of the tendons and mid-span are respectively 847 kN and 754 kN, while in the full damaged and the partial model are 854/756kN and 844/758 kN. The full damage model, given its poor bonding properties, shows lower losses in the cable and, so, higher values of the normal force. The relative displacement along the tendon shows also almost identical values. Instead, in the total traction along with the reinforcement, expected differences in the models can be observed: as expected the maximum values of shear stresses are in the grouted model with 7,18 MPa, while for the damaged and the mixed are $3{,}8 \cdot 10^{-5}$ and $-1{,}68 \cdot 10^{-5}$ MPa. In the partial model, the highest values of shear stress are located in the parts of the tendon with good bonding/grouting conditions, where the drops between different parts can be observed, while in the grouted model are located at the anchorages.

Finally, the model analysed, with different bonding properties, and configurations have shown few changes in the behaviour which were expected. The same procedure was repeated with the other 2D models, including the ones without the anchorages, and with the 3D models too.

Table 6: Results of the grouted configurations:

A	δ [mm]	P [kN]		DUSx [mm]		STSx [MPa]	
	x = 5 m	x = 5m	x = 0 / x = 10 m	x = 0 m	x = 10 m	x = 0 m	x = 10 m
Phase 1	1,28	742	850	-25,49	25,49	$-3{,}80\cdot10^{-5}$	$3{,}80\cdot10^{-5}$
Phase 2	1,28	742	839	-25,49	25,49	$-7{,}18\cdot10^{-5}$	$7{,}18\cdot10^{-5}$
	-2,98	754	847	-25,49	25,75	$-7{,}18\cdot10^{-5}$	$7{,}18\cdot10^{-5}$

Table 7: Results of the full damage configuration

B	δ [mm]	P [kN]		DUSx [mm]		STSx [MPa]	
	x = 5 m	x = 5m	x = 0 / x = 10 m	x = 0 m	x = 10 m	x = 0 m	x = 10 m
Phase 1	1,28	742	850	-25,49	25,49	$-3{,}80\cdot10^{-5}$	$3{,}80\cdot10^{-5}$
Phase 2	1,29	744	842	-25,49	25,49	$-3{,}26\cdot10^{-5}$	$3{,}26\cdot10^{-5}$
	-3,00	756	854	-25,49	25,75	$-3{,}80\cdot10^{-5}$	$3{,}80\cdot10^{-5}$

Table 8: Results of the partial damage configuration

C	δ [mm]	P [kN]		DUSx [mm]		STSx [MPa]	
	x = 5 m	x = 5m	x = 0 / x = 10 m	x = 0 m	x = 10 m	x = 0 m	x = 10 m
Phase 1	1,29	744	850	-25,54	25,54	$-3{,}80\cdot10^{-5}$	$3{,}80\cdot10^{-5}$
Phase 2	1,29	744	842	-25,54	25,54	$-0{,}85\cdot10^{-5}$	$0{,}85\cdot10^{-5}$
	-2,99	758	844	-25,54	25,54	$-1{,}68\cdot10^{-5}$	$1{,}68\cdot10^{-5}$

4.5. Cracking

4.5.1. Theory and modelling

Since the non-linear analysis carried out in the previous paragraph with the bond-slip reinforcement resulted encouraging and offered insights on the behaviour of a “damaged” tendon, it was decided to include also an analysis on cracking stage and propagation.

Concrete exhibits a complex structural response with various significant non-linearities, namely, non-linear stress-strain behaviour, tensile cracking and compression crushing material failures and creep cracking [13]. Also, since reinforced concrete shows an intricate behaviour, both elastic and plastic behaviour of concrete in compression and tension need to be accurately simulated within a finite element analysis.

Simulation of concrete under tension requires to pay particular attention to how the behaviour changes and evolves once the tensile characteristic stress is reached, in particular, tension stiffening should be included in the material model [14].

There are two main approaches to model the behaviour of concrete in the post-elastic phase, which are the discrete crack model and the smeared crack model. The discrete crack model represents the crack in the structure by disconnecting nodes between elements. This modelling is based on fracture mechanics theory and it is more suitable to capture the failure localisation. However, in this case, an adaptive re-meshing technique is required to account for the progressive failure [15]. In the smeared crack model, the effect of the cracking is smeared over

a distinct area or volume represented by each integration point in the element mesh. In Figure 12 is depicted an example of how the two approaches handle the cracking.

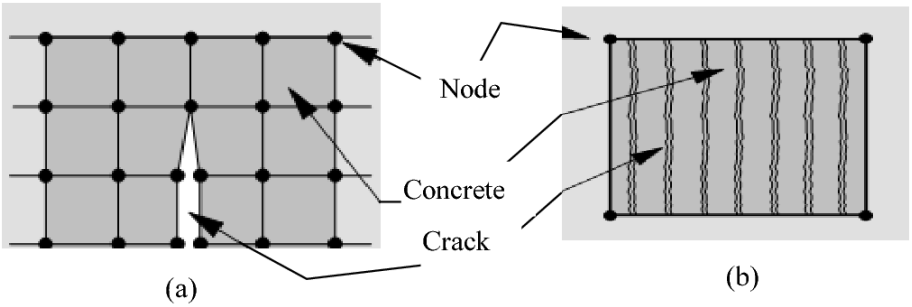

Figure 12: Cracking models: (a) discrete; (b) smeared

The discrete approach is preferred when there is one crack, or a finite number of cracks, in the structure. One of the difficulties associated with this approach is that it requires an input of material properties that are difficult to evaluate[16]. The smeared crack approach was used in this project, since the exact position of the crack is unknown, and the interest is not focused on the propagation of just one crack. The models based on the smeared approach, available in the software, are the following:

- Multiple fixed crack mode
- Total strain-based crack model, which consists of:
    - Orthogonal fixed crack model
    - Orthogonal rotating crack model
    - Switching from rotating to fixed crack model
- Rankine principal stress model

For the analysis, it was chosen, based also on previous experience and background literature, to adopt the total strain model with rotating cracks. This model is based on the Modified-Compression field theory, proposed by Vecchio and Collins [17], which assumes that the cracks grow perpendicular to the direction of the principal tensile strain. Before the cracking stage, the concrete is assumed to be isotropic and stresses and strains are calculated in the principal directions. After crack formation, the material is assumed orthotropic with the axes of the material aligned according to the condition at the crack formation [18]. Furthermore, in the rotating crack model, the rotation of the principal axes are taken into account. In this model, after the crack formation, a second crack will form as soon as the principal tensile stress exceeds the tensile strength, regardless of the direction of the stresses.

The total strain-based rotating crack model is implemented in Diana defining both the tensile and compressive behaviour of concrete. The tensile behaviour is modelled with an exponential stress-strain curve, based on the fracture energy, and related also to the crack bandwidth (Figure 13a). For the compressive behaviour, a parabolic stress-strain curve is used (Figure 13b) that depends on the compressive fracture energy. By defining a stress-strain curve in terms of the fracture energy, both for the tensile and compressive behaviour, the material becomes independent from the element size of the finite element model [19].

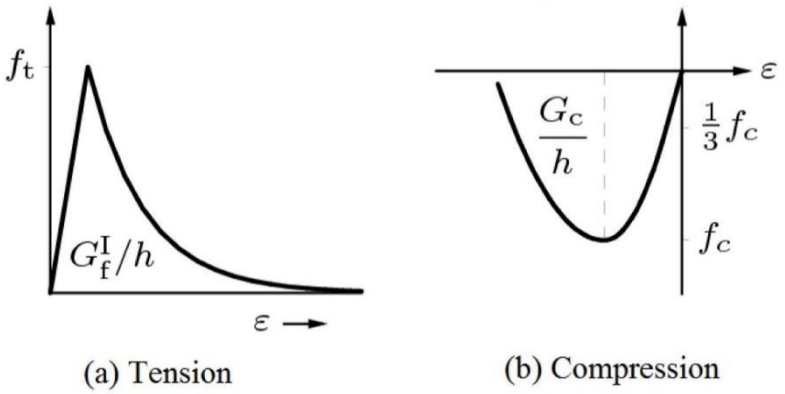

Figure 13: (a) Tensile stress-strain curve; (b) Compressive stress-strain curve

4.5.2. Numerical investigation

The model used for this part was a 2D model with one tendon and with two anchorages. The model has the same bonding properties described in the previous section. Furthermore, to avoid numerical problems during the analysis, a contact interface was created between the anchorages and the face of the beam.

The parameters needed to define the non-linear behaviour of concrete are the tensile and compressive strength and the fracture energy, both in tension [20] and compression [6], defined as in Eq. (6) and Eq. (7). Material non-linearities were given also to the prestressing cable, in particular, Von-Mises plasticity with no hardening and yield stress of 1700MPa was used.

$$Gf = 73\, fctm^{0.18} = 0.14 \frac{N}{mm} \quad \text{Eq. (6)}$$

$$Gc = 250 * Gf = 37\ \frac{N}{mm} \quad \text{Eq. (7)}$$

The analysis was performed on each model described in the previous Section: entirely bonded, unbonded and with mixed bonding conditions. A structural non-linear analysis was carried out by increasing the load. The distributed load is applied incrementally in 250 steps with a factor load of 5. The initial uniformly distributed load acting on the beam is of 1 kN/m. In this type of analysis, the arc length control was activated to follow the path of response with an automatic scale of load steps. In the arc length control settings, it was considered the translations in the Y direction because it is the direction of loading. Also, this tool requires nodes to control the analysis. For this purpose, the node at the mid-span of the beam was chosen because it is representative of the dominant displacement response. However, it is possible to choose other sets of nodes, like for instance, the nodes of a loading steel plate, if available. In the equilibrium iteration, the energy convergence norm was chosen, and the settings of the energy convergence norm were changed from terminate to continue, to allow the analysis to continue even in case of non-convergence.

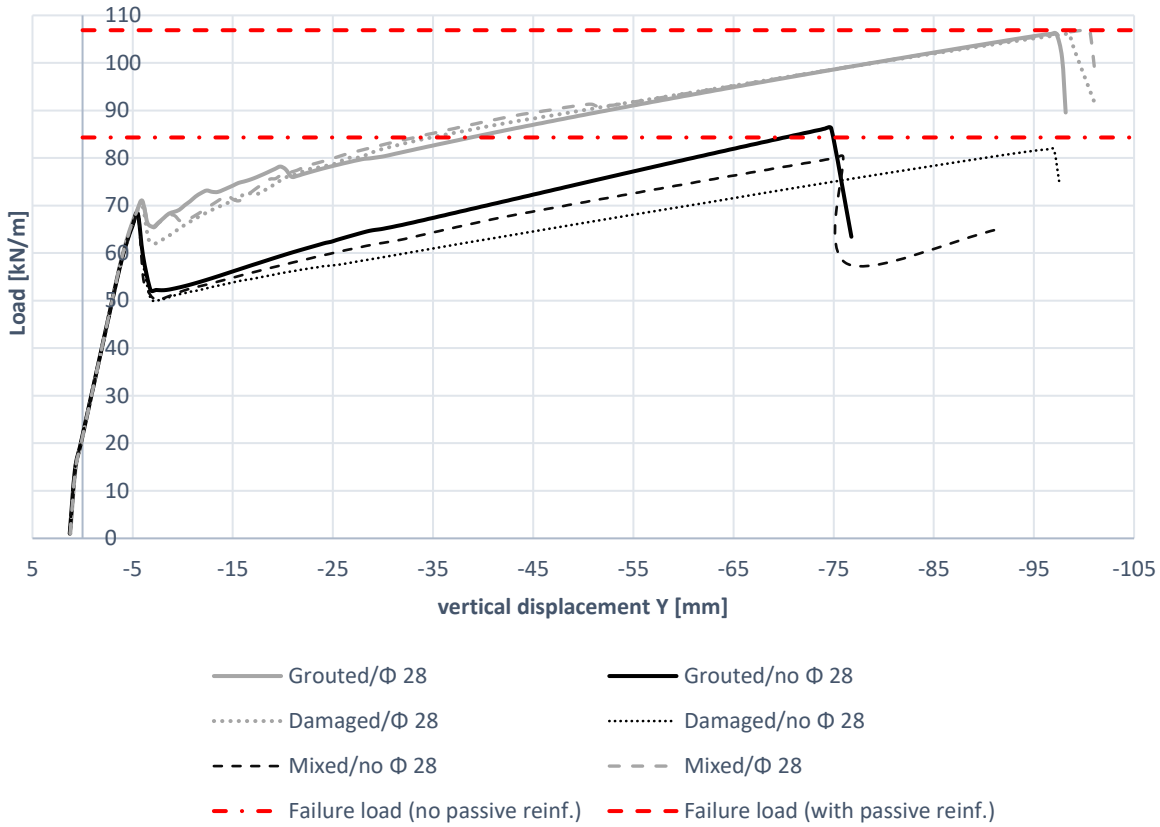

Figure 14: Load-displacement results until failure

The behaviour of the grouted, the full damaged and partial damage model until failure are displayed in Figure 14. A total of 6 curves are plotted in the graph: the grouted, damaged, and mixed model with and without passive longitudinal reinforcement. Briefly, after watching the first results of the analyses, it was decided to include two sets of reinforcement with a diameter Ø of 14 mm at d = 920 mm in the beam. This choice was forced by the fact that further explanations were needed to explain and confirm the behaviour after the first peak in the graph (models with only prestressing tendon - black lines). Being the bond-slip reinforcement, a finite element concept with uncertain parameters, many doubts arose as to whether the prestressing tendon was actually cooperating after the concrete cracked until the failure.

Thus, after adding the passive longitudinal reinforcement in the models, it was clear that the behaviour of the beam was successfully controlled by the tendon in the models with no passive reinforcement and that no numerical problems occurred. The passive reinforcement was modelled using Young's modulus of 210000 MPa, a Poisson ratio of 0,3 and yield stress of 550 MPa. It can be noted that the behaviour of the models, with the addition of the passive reinforcement, worked accordingly to the present knowledge of reinforced concrete, giving, indeed, additional capacity until failure in case of additional reinforcement while keeping a similar slope.

As expected, regardless the bonding conditions of the tendon, the beam exhibits the presence of cracking around a value of the distributed load of about 70 kN/m (corresponding to a bending moment of 75 kNm). After the peak, the behaviour of the beam is entirely reliant on the amount of reinforcement and the bonding conditions. First insight on the differences between the models can be observed in Figure 14 that shows the cracking patterns for the (a) grouted, (b)

full damage and (c) partial damage models, without passive reinforcement, at the load step immediately after the peak.

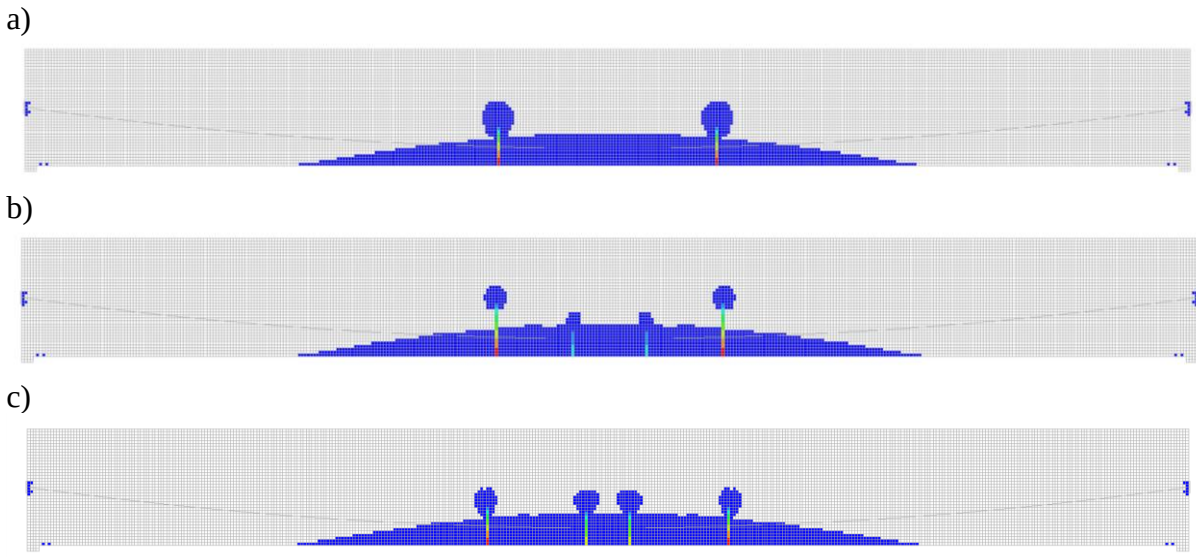

Figure 15: Load step after cracking: (a) grouted; (b) full damage; (c) partial damage

It is evident that the crack patterns are different. The cracking is more concentrated in the grouted model in two distinct cracks while more smeared in the other two models. The maximum crack width is 0.63 mm for the grouted model, 0.66 mm for the mixed and 0.43 mm for the damaged model. Even though the damaged model presents the smallest value of crack width, it has a more diffused cracking with two additional central narrow cracks. The crack formation results are in contradiction with the existing empirical and theoretical knowledge. The fully grouted solution should feature more closely spaced small cracks as opposed to the un-grouted cases that should feature fewer but larger cracks. This contradiction indicates that a revision of the crack modelling in the current models is needed.

A more consistent analysis could be performed to certificate this kind of behaviour. An iterative step by step analysis could be carried out calculating the moment of inertia J mm^4 of the cracked section and the magnitude of stress in the tendon. The position of neutral axis x and the curvature χ can be evaluated and also the other main parameters of interest such as the crack width w_k and the maximum crack spacing S_{rm}. However, even though the relationship between these parameter ceases to be linear after the cracking moment, this approximate evaluation could provide an overview of the behaviour. Further detailed analyses can nonetheless be performed.

Despite the conclusion of the previous section, in which were stated that few relevant differences between the different grouted models were found, after this cracking analysis, further considerations can be added. It can be observed from the three lower curves in Figure 14, that, as expected, the grouted and the full damage model define an upper and lower bound for the behaviour of the beam, while the partial model stands in the middle. Furthermore, in this loading step, the three models have a maximum vertical displacement of respectively 6,03mm(grouted), 6,07mm(mixed) and 6,10mm(damaged).

A reason because in the previous section were observed so slight differences between the models, could be found in the fact that until the cracking load is reached and the beam is still in the elastic stage, the models follow almost the same path. After the peak, the three models

reach the failure with different slopes (black curves in Figure 14). In particular, the grouted model (solid black) reaches the failure with a higher slope, which could be seen as a hardening behaviour, and earlier than the damaged model (black round dot) which, instead, reaches the failure at a lower load level but experiencing higher deformation (vertical displacement around 10 cm). The behaviour of the damaged model could be characterized as more ductile than the grouted one, having, in fact, a less pronounced slope.

Finally, the three highest grey curves, in Figure 14, have been calculated with the additional passive longitudinal reinforcement. The behaviour of the models seems to be similar, except for several load step after the peak in which the differences between the curve are the same stated previously.

The models have also proven to work according with the analytical calculations. A design check for the ultimate limit state has been carried out. The calculation of the failure load was done with unitary material and load safety factors, giving as final result for the grouted model, with and without passive longitudinal reinforcement, respectively 85 kN/m (M_u=1054 kNm) and 107 kN/m (M_u=1336 kNm). In Figure 14, the failure loads are depicted by the two red lines. The response of the finite element model seems to be satisfactory, reaching, in fact the collapse around the failure load calculated analytically.

5. Conclusions

The result of this work helped to better understand the behaviour of a post-tension concrete structure affected by damage, where damage is defined as missing grout. The damaged model with poor bonding properties shows differences in terms of capacity and deformability. A partial damaged situation has proven to be effective, but more studies are recommended, especially in the elastic stage, to really observe its nature.

The development of these models needs also to consider the passive reinforcement. As showed in the numerical analysis there is a relevant change in the behaviour when the reinforcement is added into the structure. It could be interesting to study in more detail what is the limit amount of passive reinforcement beyond which the structure is not affected by the poor bonding properties of the tendons, and, especially, what could be the outcomes of different amounts of reinforcement on the structure.

Different cracking patterns have also been observed between the models with different grouting conditions. However, the results contradict empirical experiences, therefore indicating that the adopted crack modelling approach must be revised. More insights can be obtained by working more closely and analysing real structures affected by these kinds of damages. It can be stated that the response of the presented finite element models with the bonding and non-linear material properties is satisfactory regarding displacement behaviour and maximum load bearing capacities.

Further works could be carried out including the influence of the corrosion and the long-term properties of concrete (creep and shrinkage). Finally, additional 3D analyses are suggested to confirm and further investigate the influence of the different bonding properties on a post-tension concrete structure.

References

[1] S. Hurlebaus *et al.*, *Inspection Guidelines for Bridge Post-Tensioning and Stay Cable Systems Using NDE Methods*. Washington, D.C.: Transportation Research Board, 2017, p. 24779.

[2] "Parameters Influencing Corrosion and Tension Capacity of Post-Tensioning Strands," *ACI Mater. J.*, vol. 106, no. 2, 2009, doi: 10.14359/56461.

[3] "'CEN. EN 1992-1-1, Eurocode 2: Design of Concrete Structures—Part 1-1: General Rules and Rules for buildings. Brussels: European Committee for Standardization; 2004.' ." .

[4] Y. Huang and T. H.-K. Kang, "Modeling of Sliding Behavior of Unbonded Tendons in Post-Tensioned Concrete Members," *ACI Struct. J.*, vol. 115, no. 4, Jul. 2018, doi: 10.14359/51702066.

[5] "DIANA FEA BV (2020), DIANA User's Manual, Manie, J." .

[6] "Max A.N. Hendriks and Marco A. Roosen (editors), 'Guidelines for Nonlinear Finite Element Analysis of Concrete Structures', Rijkswaterstaat Centre for Infrastructure, Report RTD:1016- 1:2019, 2019.," *Concr. Struct.*, p. 66, 2020.

[7] *CEB-FIP. CEB-FIP Model Code 1990. Comité Euro-International du Béton, 1993*. Thomas Telford Publishing, 1993.

[8] M. Eriksen and M. Kolstad, "Investigation of Cracking Behavior in Reinforced Concrete Panels with Bond-slip Reinforcement," p. 166.

[9] "What is the guideline for reasonable choice values of tangent and normal stiffness of interface elements? | DIANA FEA." https://dianafea.com/faq-tangent-normal-stiffness (accessed Jan. 05, 2021).

[10] R. I. Gilbert, N. C. Mickleborough, and G. Ranzi, "Design of Prestressed Concrete to Eurocode 2, Second Edition," p. 700.

[11] *NAFEMS. Guidelines to Finite Element Practice. National Agency for Finite Element Methods & Standards (NAFEMS), Glasgow, 1984.* .

[12] C.-H. Jeon, C. D. Nguyen, and C.-S. Shim, "Assessment of Mechanical Properties of Corroded Prestressing Strands," *Appl. Sci.*, vol. 10, no. 12, Art. no. 12, Jan. 2020, doi: 10.3390/app10124055.

[13] K.-J. Bathe and et al, *Nonlinear Analysis of Concrete Structures*. 1989.

[14] P. Gianclaudio, "Structural analysis of long-span suspension bridge top tower: Application of Non-linear finite element analysis," NTNU, 2019.

[15] L. Jendele and E. Consulting, "On the choice between discrete or smeared approach in practical structural FE analyses of concrete structures," p. 18.

[16] J. C. Gálvez, J. Červenka, D. A. Cendón, and V. Saouma, "A discrete crack approach to normal/shear cracking of concrete," *Cem. Concr. Res.*, vol. 32, no. 10, pp. 1567–1585, Oct. 2002, doi: 10.1016/S0008-8846(02)00825-6.

[17] F. J. Vecchio and M. P. Collins, "The Modified Compression-Field Theory for Reinforced Concrete Elements Subjected to Shear," p. 13, 1986.

[18] J. G. Rots and J. Blaauwendraad, "Crack Models for Concrete, Discrete or Smeared? Fixed, Multi-Directional or Rotating?," *HERON 34 1 1989*, 1989, Accessed: Jan. 18, 2021. [Online]. Available: https://repository.tudelft.nl/islandora/object/uuid%3A0a401939-2938-4f9d-a395-b6a6652b2cd9.

[19] P. J. van der Aa and A. A. van den Bos, "Material Characterisation for Nonlinear Finite Element Analysis (NLFEA)," in *Fibre Reinforced Concrete: Improvements and Innovations*, Cham, 2021, pp. 503–514, doi: 10.1007/978-3-030-58482-5_46.

[20] International Federation for Structural Concrete, Ed., *Model Code 2010: final draft. Vol. 1:* ... Lausanne: International Federation for Structural Concrete, 2012.

NTNU
Norwegian University of
Science and Technology